Structure Preserving Denoising of SAR Images using Multifractal Feature Analysis

Suman Kumar Maji, Ramesh Kumar Thakur and Hussein M. Yahia

***Abstract*—In this paper, we propose a speckle removal denoising algorithm for synthetic aperture radar (SAR) images. The approach is based on the concept of extracting informative feature (based on the concept of multifractal decomposition of signals) from a speckle induced SAR image, and then estimating a noise free image from the gradients restricted to those features. Experimental results show that the proposed technique not only improves the visual quality of the SAR images but also effectively preserves their texture. Comparison with classical and state-of-the-art denoising techniques shows the advantages of the proposed scheme, both visual and quantitative.**

***Index Terms*—Image denoising, speckle noise, synthetic aperture radar (SAR) images, multifractal exponents.**

I. Introduction

SYNTHETIC aperture radar (SAR) is a widely used technology for acquiring landscape images from high altitude reconnaissance aircrafts or low altitude spacecrafts. The acquired images, however, suffer from the effect of noise due to random phase fluctuations introduced in the signal during its acquisition. The induced noise is multiplicative in nature and referred to as speckle noise. Image interpretation ability from acquired SAR images is severely limited due to the presence of speckle noise which poses a challenge to the application of this technology. Speckle removal or speckle denoising is therefore a widely investigated area, actively pursued by researchers, in the field of geoscience and remote-sensing as well as medical ultrasound imaging.

As early as in 1980, a computational model for multiplicative noise filtering was proposed in [1]. In 1987 a more refined model was proposed in [2], where a local linear minimum mean square error (LMMSE) filter was designed, taking into account statistical information of the speckle noise during image formation. A PDE-based speckle removal model was proposed in [3]. This method, known as the speckle reducing anisotropic diffusion filter or SRAD, is an edge preserving diffusion filter based on the MMSE estimator. In [4], the authors propose a speckle removal filter known as the Iterative Probabilistic Patch-Based filter or PPBit. The method is based on a weighted maximum-likelihood estimator where the weights are refined, from image patches, in an iterative framework to generate best possible result. Wavelet-based denoising methods [5], [6] have also been investigated in the area of SAR image denoising. These methods allow significant noise reduction as well as detail preservation, owing to the sparse representation of the signal in the transformed domain. The modified version of the block matching 3D algorithm (BM3D) [7] known as SAR-BM3D [8], which is based on the concepts of non-local filtering and wavelet shrinkage, is a very popular denoising method in this regard.

In this paper, we propose a feature extraction based gradient domain image reconstruction model for SAR image denoising. Given a noisy SAR image, we first compute, at each pixel of the image, the value of the singularity exponent of a measure defined by the density of the signal gradient's norm. Then through a hierarchical decomposition process over these exponents, we extract a set of pixels which encodes only the sharpest transitions of the image and discards the background noise. This set of pixel serve as our most informative feature set. Information of the gradients over these extracted features are then used to reconstruct a noise suppressed clean (denoised) image. An overview of the procedure is shown in fig. 1.

II. Multifractal Systems and Feature Extraction

Natural scale-free systems are in general self-similar and of multifractal nature [10], which means that measurements signals acquired out of these systems display power-law behaviour which express self-similarity. This is particularly true for natural images which are often in the form of 2D acquisitions of intensive physical variables. Let $z(\mathbf{x})$ be such an image, in our case the observed noisy SAR image, where $\mathbf{x} = (x, y)$ is a 2D pixel location, and let us consider the projections of the gradient's norm $\|\nabla z\|$ at different scales r and at each position $\mathbf{x}$ as:

$$\mathbb{T}_\psi(\|\nabla z\|)(\mathbf{x}, r) = \int \|\nabla z\|(\mathbf{y}) \frac{1}{r^d} \psi(\frac{\mathbf{x}-\mathbf{y}}{r}) \mathrm{d}\mathbf{y}, \quad (1)$$

where ψ is a mother wavelet and d is the dimension of the signal domain ($d = 2$ for images). When the signal z is multifractal, one has the limiting behaviour [11], [12], [13]:

$$\mathbb{T}_\psi(\|\nabla z\|)(\mathbf{x}, r) = \alpha(\mathbf{x}) r^{h(\mathbf{x})} + o(r^{h(\mathbf{x})}) \quad (r \to 0) \quad (2)$$

where $\alpha(\mathbf{x})$ is a signal dependent amplitude prefactor. The exponent $h(\mathbf{x})$, which is a function of the point $\mathbf{x}$, is called the *singularity exponent* at point $\mathbf{x}$. The term $o(r^{h(\mathbf{x})})$ is a quantity that decreases to zero faster than $r^{h(\mathbf{x})}$ and hence can be neglected to small values of r. Taking log on both sides, equation (2) then takes the form:

$$\mathbb{T}_\psi(\|\nabla z\|)(\mathbf{x}, r) = \log(\alpha(\mathbf{x})) + h(\mathbf{x}) \log r \quad (r \to 0) \quad (3)$$

Suman Kumar Maji is with the Department of Computer Science & Engineering, Indian Institute of Technology Patna, 801103 Patna, India (Email:smaji@iitp.ac.in).

Ramesh Kumar Thakur is with the Department of Computer Science & Engineering, Indian Institute of Technology Patna, 801103 Patna, India (Email:ramesh.pcs17@iitp.ac.in).

Hussein Yahia is with the Geostat team (Geometry and Statistics in Acquisition Data: http://geostat.bordeaux.inria.fr) of INRIA, 200 rue de la Vieille Tour, 33405 Talence Cedex, France (Email: hussein.yahia@inria.fr).

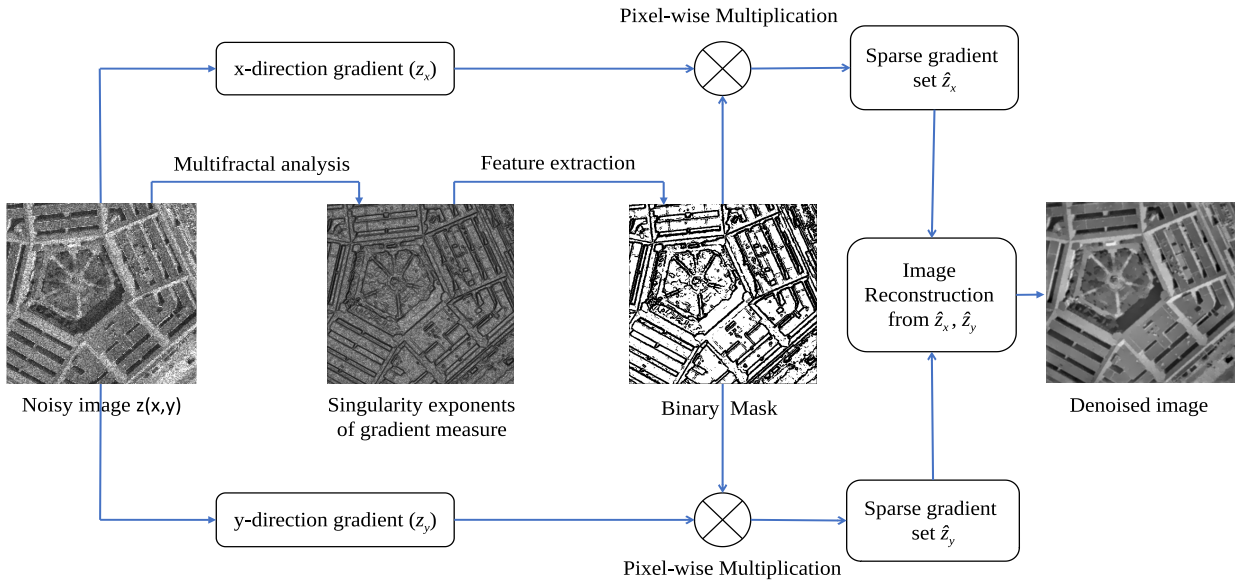

Fig. 1: **Block diagram of the proposed denoising algorithm:** We consider the Pentagon image from the SIPI image database [9]. The image is corrupted with simulated speckle to generate the case of a SAR acquisition. Multifractal exponents are then computed over this noisy image and the features extracted. Finally a denoised image is generated from the information of the gradients restricted to these features.

Consequently, the limiting quantity $h(\mathbf{x})$ can be estimated through $\log - \log$ regression from a set of scales and pixel values as is described below. The preferred wavelet of choice is the β-Lorentzian wavelet which are isotropic wavelets and therefore do not privilege any particular direction [13]:

$$\psi(\mathbf{x}) = \psi^{\beta}(\mathbf{x}) = \frac{1}{(1+|\mathbf{x}|^2)^{\beta}} \quad (\text{for } \beta = 1,2,3,4), \tag{4}$$

For multiple values of $r, r = \{r_0, r_1, \cdots, r_n\}$ and a given pixel $\mathbf{x}$, equation (3) can be written as:

$$\begin{array}{rcl} \log(\mathbb{T}_\psi(\|\nabla z\|)(\mathbf{x}, r_0)) & = & \log(\alpha(\mathbf{x})) + h(\mathbf{x})\log(r_0) \\ \log(\mathbb{T}_\psi(\|\nabla z\|)(\mathbf{x}, r_1)) & = & \log(\alpha(\mathbf{x})) + h(\mathbf{x})\log(r_1) \\ \vdots & = & \vdots \quad + \quad \vdots \\ \log(\mathbb{T}_\psi(\|\nabla z\|)(\mathbf{x}, r_n)) & = & \log(\alpha(\mathbf{x})) + h(\mathbf{x})\log(r_n) \end{array} \tag{5}$$

and can be expressed in the matrix framework as:

$$\begin{bmatrix} \log(\mathbb{T}_\psi(\|\nabla z\|)(\mathbf{x}, r_0)) \\ \log(\mathbb{T}_\psi(\|\nabla z\|)(\mathbf{x}, r_1)) \\ \vdots \\ \log(\mathbb{T}_\psi(\|\nabla z\|)(\mathbf{x}, r_n)) \end{bmatrix} = \begin{bmatrix} 1 & \log(r_0) \\ 1 & \log(r_1) \\ \vdots & \vdots \\ 1 & \log(r_n) \end{bmatrix} \times \begin{bmatrix} \log(\alpha(\mathbf{x})) \\ h(\mathbf{x}) \end{bmatrix} \tag{6}$$

If N is the number of pixels in a given image, then considering all the pixels $\{x_0, x_1, \cdots, x_{N-1}\}$ and rewriting the above equation allows us to calculate all the exponents at once by solving the following linear system in the unknown y:

$$\underbrace{\begin{bmatrix} \log(\mathbb{T}_\psi(\|\nabla z\|)(\mathbf{x}, r_0)) & \cdots & \log(\mathbb{T}_\psi(\|\nabla z\|)(\mathbf{x_{N-1}}, r_0)) \\ \log(\mathbb{T}_\psi(\|\nabla z\|)(\mathbf{x}, r_1)) & \cdots & \log(\mathbb{T}_\psi(\|\nabla z\|)(\mathbf{x_{N-1}}, r_1)) \\ \vdots & \cdots & \vdots \\ \log(\mathbb{T}_\psi(\|\nabla z\|)(\mathbf{x}, r_n)) & \cdots & \log(\mathbb{T}_\psi(\|\nabla z\|)(\mathbf{x_{N-1}}, r_n)) \end{bmatrix}}_{b} =$$

$$\underbrace{\begin{bmatrix} 1 & \log(r_0) \\ 1 & \log(r_1) \\ \vdots & \vdots \\ 1 & \log(r_n) \end{bmatrix}}_{A} \times \underbrace{\begin{bmatrix} \log(\alpha(\mathbf{x_0})) & \cdots & \log(\alpha(\mathbf{x_{N-1}})) \\ h(\mathbf{x_0}) & \cdots & h(\mathbf{x_{N-1}}) \end{bmatrix}}_{y} \tag{7}$$

Equation (7) can be solved by minimizing $\|Ay - b\|_2^2$ in the l^2 norm using Least squares:

$$\arg\min_{y} \|Ay - b\|_2^2 \quad \text{with} \quad h(\mathbf{x}_i) = y(2,i) \tag{8}$$

Once the singularity exponents $h(\mathbf{x})$ are computed for every pixel $\mathbf{x}$ they define a *multifractal hierarchy* associated with the fractal sets $\mathcal{F}_h$ as:

$$\mathcal{F}_h = \{\mathbf{x} : h(\mathbf{x}) = h\} \tag{9}$$

with the set $\mathcal{F}_\infty$, comprising of components associated to the smallest possible value h_∞, as:

$$\mathcal{F}_\infty = \{\mathbf{x} : h(\mathbf{x}) = h_\infty = \min(h(\mathbf{x}))\} \tag{10}$$

The procedure for calculating $\mathcal{F}_\infty$ is summarized in algorithm 1. The set $\mathcal{F}_\infty$ encodes only those pixels that correspond to sharp transitions in the image and reveals a structure similar to edges or contours in an image. When applied over noisy SAR images, $\mathcal{F}_\infty$ maintains its stability in recording the sharp transition pixels of the images while simultaneously eliminating the background noise, as shown in fig. 1.

Algorithm 1 Determining $\mathcal{F}_\infty$

Step 1: Normalize the noisy SAR image $z(\mathbf{x})$ using image mean subtraction : $z(\mathbf{x}) - \langle z(\mathbf{x}) \rangle$.
Step 2: Compute the multifractal exponents $h(\mathbf{x})$ of image $z(\mathbf{x})$.
Step 3: h_∞ is calculated as the average of $h(\mathbf{x})$ corresponding to 1% and 5% quantiles.
Step 4: The dispersion Δh around h_∞ is conventionally fixed (± 0.2 is usually a good choice).
Step 5: Define a density function $\delta_{\mathcal{F}_\infty}$ as: $\delta_{\mathcal{F}_\infty}(\mathbf{x}) = 1$ if $h_\infty - \Delta h \leq h(\mathbf{x}) \leq h_\infty + \Delta h$ and $\delta_{\mathcal{F}_\infty}\mathbf{x}) = 0$ otherwise.
Step 6: $\delta_{\mathcal{F}_\infty}(\mathbf{x})$ is a binary mask that locates the $\mathcal{F}_\infty$ pixels.

III. Reconstruction from Extracted Features

In this section, we explain the procedure of reconstructing a denoised image from the binary mask $\delta_{\mathcal{F}_\infty}$ (refer to Algorithm 1), corresponding to the extracted feature set $\mathcal{F}_\infty$. If $\{z_x, z_y\}$ are the gradients of the noisy image z, then our objective is to estimate a smooth surface from the sparse gradient set $\hat{z_x} = z_x \cdot \delta_{\mathcal{F}_\infty}$, $\hat{z_y} = z_y \cdot \delta_{\mathcal{F}_\infty}$. Since $\mathcal{F}_\infty$ encodes the most informative features of the image, the gradients restricted to its pixels will the most informative and least corrupted gradients of the image. A surface estimated from this sparse gradient set $\{\hat{z_x}, \hat{z_y}\}$ will therefore be a denoised image.

If $\{s_x, s_y\}$ are the gradients of the clean image s, we propose to minimize the following optimization problem:

$$\hat{s} = \underset{s}{\operatorname{argmin}} \int\int ((s_x - \hat{z_x})^2 + (s_y - \hat{z_y})^2 + \lambda(\phi(s_x) + \phi(s_y)))dxdy \tag{11}$$

where λ is the general regularization parameter and ϕ a functional. Solving the above equation using Euler-Lagrange gives us:

$$\text{div}(s_x, s_y) + \frac{\lambda}{2}\text{div}(\phi'(s_x), \phi'(s_x)) = \text{div}(\hat{z_x}, \hat{z_y}) \tag{12}$$

Considering $\phi(\cdot) = \| \cdot \|_2^2$, reduces the above equation to:

$$(1 + \lambda)\text{div}(s_x, s_y) = \text{div}(\hat{z_x}, \hat{z_y}) \tag{13}$$

Taking Fourier transform on both sides and simplifying, we get:

$$s(\omega) = -i\frac{\omega_x \mathcal{F}(\hat{z_x}) + \omega_y \mathcal{F}(\hat{z_y})}{(1 + \lambda)(\omega_x^2 + \omega_y^2)} \tag{14}$$

where $\mathcal{F}$ denotes the Fourier transform. Fourier inversion of this formula gives us the denoised image $\hat{s}$, obtained from the sparse gradient set $\{\hat{z_x}, \hat{z_y}\}$, as:

$$\hat{s} = \mathcal{F}^{-1}\{s(\omega)\} \tag{15}$$

The results of reconstruction over test images are shown in fig.2 and on real SAR data in fig. 3,4 respectively.

TABLE I: Quantitative evaluation of synthetic images (best values in boldface).

Metric	Methods	Number of looks (L)				
		L = 1	L = 2	L = 4	L = 8	L = 16
PSNR	Proposed	**21.2822**	**22.7194**	**23.5958**	**24.2715**	**24.4067**
	SAR-BM3D	20.0542	20.9992	21.8885	22.6900	23.5783
	PPBit	19.7193	20.0017	21.1883	21.9837	22.5654
	SRAD	18.4932	18.9838	19.4908	20.3323	20.7567
SSIM	Proposed	**0.8316**	**0.8551**	**0.8783**	**0.9006**	**0.9315**
	SAR-BM3D	0.8176	0.8297	0.8529	0.8750	0.8900
	PPBit	0.7589	0.7689	0.7721	0.7724	0.7727
	SRAD	0.7464	0.8165	0.8466	0.8380	0.8348
FOM	Proposed	**83.6707**	**88.0752**	**91.8342**	**93.4444**	**94.7047**
	SAR-BM3D	81.7294	80.9111	84.8156	87.6973	88.5596
	PPBit	75.9090	74.7723	74.2397	74.2474	74.5898
	SRAD	72.2415	85.6734	84.5208	82.4646	81.1909

IV. Results & Discussion

In order to validate the potential of the proposed technique, we compare it with the following methods: PPBit filter [4] , SRAD filter [3] and SAR-BM3D [8]. A brief overview of these techniques are provided in section I. We have used synthetic test image as well as real SAR images for our experiments.

A. Synthetic Data

We have used the Pentagon image (512×512 pixels) from the SIPI image database [9]. We add simulated multiplicative speckle noise to this image and test using the above mentioned methods.

In Fig. 2, we show the qualitative results over the Pentagon image. By visual observation, it is clear that both SAR-BM3D and proposed technique gives better denoising results than the other techniques. However, the proposed technique supersedes SAR-BM3D in terms of feature preservation. The finer details on the roof structure are well preserved by the proposed denoising technique and are mostly lost in SAR-BM3D, which fails to preserve them due to over smoothing. Excessive smoothing is also observed in the case of PPBit and SRAD which results in the formation of blurred images.

For quantitative analysis, we have considered the peak signal-to-noise ratio (PSNR, expressed in dB), structural similarity index metric(SSIM) and Pratt's figure of merit(FOM) metrics. Results of the different comparing algorithms, for single-look as well as multi-look speckle ($L = 1, 2, 4, 8, 16$) are shown in table I. It is observed that the proposed algorithm gives the best denoising result (over the other existing techniques) in terms of PSNR, SSIM and FOM.

B. Real SAR Images

We have considered two real world SAR images for our experiments, as is discussed in the following subsections.

1) Oil Rig explosion SAR image: We have considered the the Pléiades Satellite Image - Oil Rig explosion "Permanent Abkatun", Gulf of Mexico as one of our real SAR images. The white area shows the spilled oil region over the ocean and the crossed structures are the oil rigs. The image is a

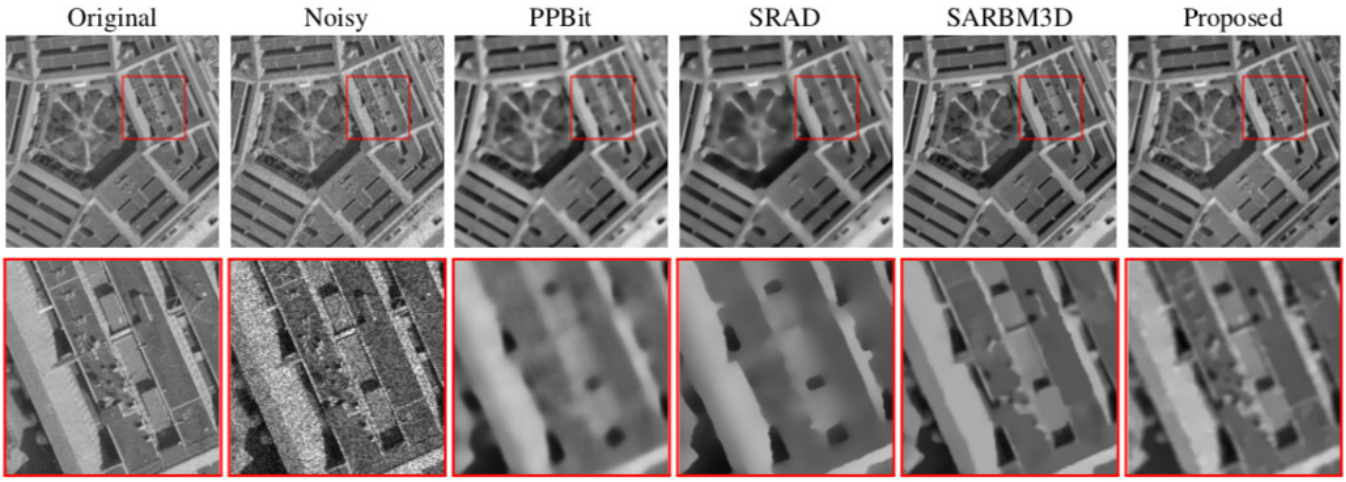

Fig. 2: **Denoising result over synthetic image. From left to right: Row 1** Original image, noisy image, denoised outputs of PPBit, SRAD, SARBM3D and proposed. **Row 2:** Excerpts from row 1 highlighted in red.

TABLE II: Quantitative evaluation of real images for selected ROIs (best values in boldface).

Image	**Methods**	**ROI-1**			**ROI-2**		
		ENL	μ_r	ENL_r	ENL	μ_r	ENL_r
OilRig-Explosion	Proposed	**846.8100**	**1.0097**	**3.6488**	**172.3277**	**0.9713**	1.5308
	SAR-BM3D	346.5600	0.9670	4.5583	108.6658	0.8048	**1.2848**
	PPBit	339.8116	0.9346	4.7450	167.8841	0.7000	6.5474
	SRAD	767.2900	1.0605	4.5411	147.2356	0.9465	3.1830
ThreeGo-rgesDam	Proposed	$\mathbf{1.1395\times10^3}$	**0.9878**	**5.0422**	**399.5272**	**1.0167**	**2.7127**
	SAR-BM3D	482.9938	0.8922	5.8626	192.6567	0.8517	3.3302
	PPBit	389.5833	0.9274	6.0415	126.0134	0.9335	3.3659
	SRAD	712.0385	0.9746	5.6699	84.2022	0.9811	2.9862

highly textured image due to ocean waves and shows sufficient presence of noise in it. Denoising has been done over this image.

In fig. 3, we present the denoising outputs over this data. Row 1 shows the denoising results over the whole image, while row 2 shows the result over the excerpt. The proposed method clearly gives the best denoising results while preserving the texture as well as the ocean wave structures. PPBit filter also try to preserve these details, but fails to retain the image sharpness at par with the proposed method. SRAD filter retains texture at certain regions while over-smoothing the rest, thereby giving unpleasant denoising result. SAR-BM3D removes noise at the expense of introducing heavy blur, thereby loosing all fine details of the image.

2) Three Gorges Dam SAR image: The second image is the TerraSAR-X acquisition of Three Gorges Dam, China. This image is an acquisition of a hilly region with a water body (river) flowing through it. We choose one excerpt from this image: the red boundary region shows the hilly region with the sharp cuts. This image is also highly textured (due to the rugged mountainous terrain) and have sufficient noise.

In fig. 4 we present the denoised output. SRAD denoising is less blurry but suffers from artefacts due to uneven smoothing. PPBit and SAR-BM3D produces comparatively better results, but looses the finer details of the terrain due to over smoothing. The proposed technique gives the best denoising result over the others. The rugged terrain texture is well retained while over smoothing and blurring is negligible, thereby achieving clear visible superiority in terms of denoising.

For quantitative analysis of real images, we have considered the equivalent number of looks of denoised image (denoted as ENL), mean value of ratio image (denoted as μ_r) and equivalent number of looks of ratio image (denoted as ENL_r) for two region of interest (denoted as ROI 1 and ROI 2 in white boundary in fig. 3 and fig. 4). Results of the different comparing algorithms for two ROI's are shown in table II. It is quite clear from the table that the proposed algorithm gives the best denoising result (over the other existing techniques) in terms of ENL, μ_r and ENL_r.

V. Conclusion

In this paper, we have proposed a feature extraction based image denoising technique for speckle corrupted SAR images. The proposed approach is based on the concept of multi-fractal feature extraction and subsequent noise elimination. The gradients restricted to the extracted features are the most informative and hence least corrupted gradients of the image. Reconstruction from these gradients therefore generates a denoised version of the whole image. We have shown extensive experimental results both on synthetic as well as real SAR images. For synthetic image, we have validated the performance of the proposed technique qualitatively and quantitatively, against multiple state-of-the-art as well as classical SAR denoising techniques. We have then demonstrated the performance of our algorithm over real world SAR images. Results show that the proposed technique maintains the finer details of the surface while denoising unlike the rest of the algorithms, which looses these detail due to over smoothing and blurring, thereby justifying its superiority over some well known competing algorithms.

Acknowledgment

This work is supported by a SERB Early Career Research Award (ECR/2017/000896) grant.

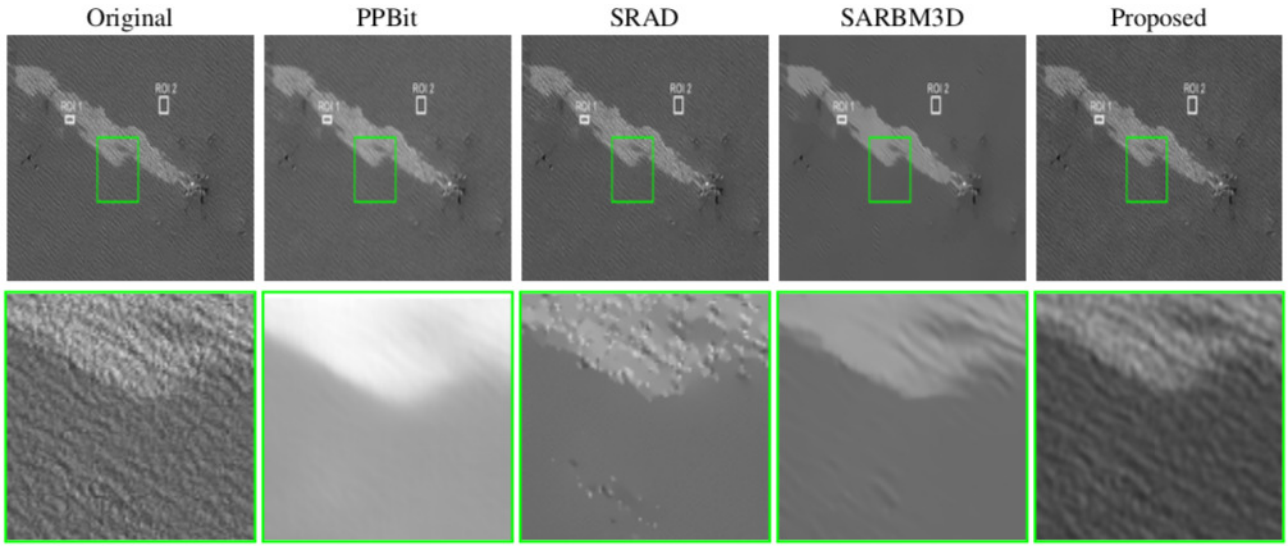

Fig. 3: **Denoising results over Oil Rig explosion SAR image. From left to right: Row 1** Original image, denoised outputs of PPBit, SRAD, SARBM3D and proposed. **Row 2:** Excerpts from row 1 highlighted in green.

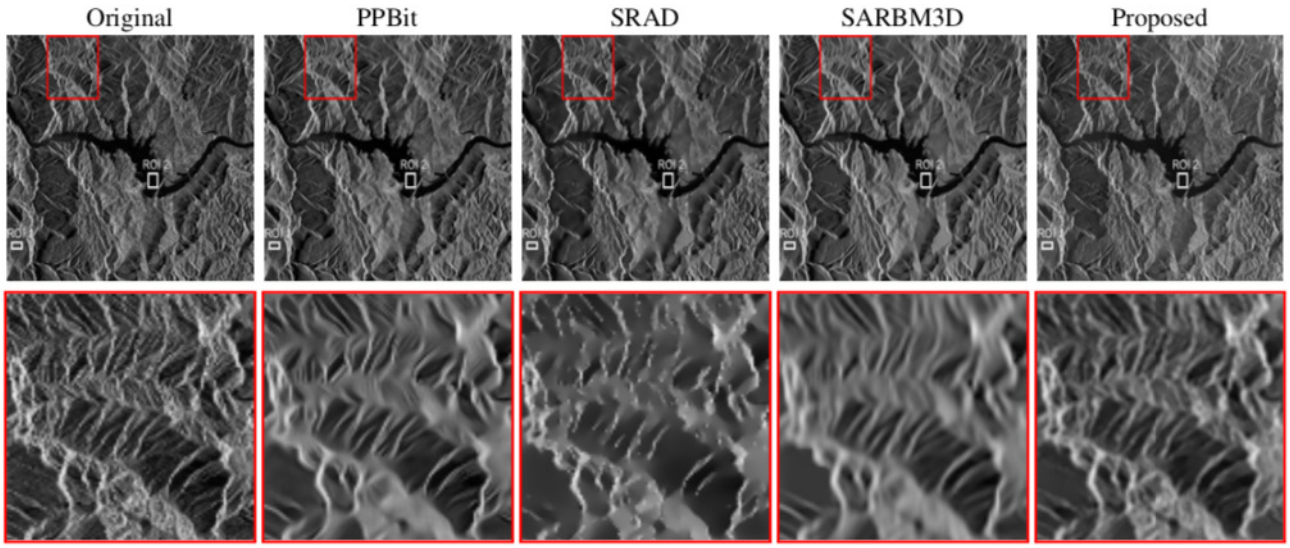

Fig. 4: **Denoising result over Three Gorges Dam SAR image. From left to right: Row 1** Original image, denoised outputs of PPBit, SRAD, SARBM3D and proposed. **Row 2:** Excerpts from row 1 highlighted in red.

REFERENCES

[1] J.S. Lee, "Digital image enhancement and noise filtering by using local statistics," *IEEE Trans. Pattern Anal. Mach. Intell.*, vol. 2, pp. 165–168, 1980.

[2] T. Strand D. Kuan, A. Sawchuk and P. Chavel, "Adaptive restoration of images with speckle," *IEEE Trans. Acoust., Speech Signal Process.*, vol. 35, no. 3, pp. 373–383, 1987.

[3] S.T. Acton Y. Yongjian, "Speckle reducing anisotropic diffusion," *IEEE Trans. Image Process.*, vol. 11, pp. 1260–1270, 2002.

[4] L. Denis C. A. Deledalle and F. Tupin, "Iterative weighted maximum likelihood denoising with probabilistic patch-based weights," *IEEE Trans. Image Process.*, vol. 18, no. 12, pp. 2661–2672, 2009.

[5] Qingwei Gao, Yanfei Zhao, and Yixiang Lu, "Despeckling sar images using stationary wavelet transform combining with directional filter banks," vol. 205, pp. 517–524, 11 2008.

[6] S. Parrilli, M. Poderico, C. V. Angelino, and L. Verdoliva, "A nonlocal sar image denoising algorithm based on llmmse wavelet shrinkage," *IEEE Transactions on Geoscience and Remote Sensing*, vol. 50, no. 2, pp. 606–616, Feb 2012.

[7] V. Katkovnik A. Danielyan, A. Foi and K. Egiazarian, "Image denoising by sparse 3d transform-domain collaborative filtering," *IEEE Trans. Image Process.*, vol. 16, no. 8, pp. 2080–2095, 2007.

[8] C. V. Angelino S. Parrilli, M. Poderico and L. Verdoliva, "A nonlocal sar image denoising algorithm based on llmmse wavelet shrinkage," *IEEE Trans. Geosci. Remote Sens.*, vol. 50, no. 2, pp. 606–616, 2012.

[9] "USC-SIPI image database," http://sipi.usc.edu/database/, 1981.

[10] K. Falconer, *Techniques in fractal geometry*, John Wiley, 1997.

[11] A. Turiel and N. Parga, "The multifractal structure of contrast changes in natural images: From sharp edges to textures," *Neural Computation*, vol. 12, pp. 763–793, 2000.

[12] A. Turiel, H. Yahia, and C. J. Pérez-Vicente, "Microcanonical multifractal formalism -a geometrical approach to multifractal systems: Part 1. singularity analysis," *J. Phys. A: Math. Theor.*, vol. 41, no. 015501, 2008.

[13] A. Turiel, C. J. Pérz-Vicente, and J. Grazzini, "Numerical methods for the estimation of multifractal singularity spectra on sampled data: A comparative study," *Journal of Computational Physics*, vol. 216, pp. 362–390, 2006.